Supporting Information

Khodakovskaya et al. 10.1073/pnas.1008856108

SI Text

Photothermal and Photoacoustic Plant Mapping. ***Sample preparation.*** The plants tested were extracted from the Murashige and Skoog (MS) medium and washed with phosphate-buffer solution (PBS) at least five times to remove multiwall carbon nanotubes (CNTs). For testing convenience, parts of the sample—such as a whole leaf or root—were detached from the main plant body and gently pressed between a glass slide and thin coverslip with PBS added as the medium for ultrasound propagation. In general, the same procedure could be repeated with intact leaves connected to the plant body. An ultrasonic transducer was placed flat atop the thin coverslip at 4–6 μm lateral distance from the laser spot with a conventional ultrasound gel used for acoustic matching. The thickness of the sample was ~0.4 mm for a leaf and ~0.1 mm for a root.

Measuring procedure. PA/PT imaging. Some of the leaves were dried between glass slides to improve their optical quality. PBS solution was added on the first day to preserve the sample. Light steady pressure was applied to these samples during drying. The dried leaves were ~0.1 mm thick. Other than a decrease in leaf light scattering, there were no changes in sample coloring or deformation of cells observed.

Areas of the sample to be tested were selected visually to avoid damaged portions. Before and after each scan, transmission images were recorded and compared (at 20× and 60× magnification) to control photodamage of the sample. Distribution of light absorbing components in the sample was mapped by photoacoustic (PA) and photothermal (PT) modalities with 10 μm stepping at laser wavelength of 903 nm. Forty PA/PT signals were recorded and averaged for each step to improve detection sensitivity. The same procedure with 740 nm excitation wavelength was used to selectively destroy chlorophyll b in the sample to reveal the structure of vessels.

PA spectroscopy. In PA spectroscopy mode (Fig. 2*B*, PA spectra of plants and of the CNTs in model sample), the PA signals at different wavelengths of the optical parametric oscillator (OPO) were acquired from the same point of the sample. 100 PA signals were averaged for each laser wavelength; the spectral range was automatically scanned by OPO with a 5 nm step. The total analysis duration was less than 3 min. Peak-to-peak amplitudes of the averaged PA signals were used to construct a PA spectrum of the sample. PA spectra of the green and nongreen tomato leaves were calculated as an average of seven spectra taken from different parts of the leaf (Fig. 2*B*).

PT spectroscopy. In PT spectroscopy mode, images were acquired at different wavelengths from the same small sample area (50 × 50 μm, 5 μm step size). For CNTs in tomato, PT signal amplitudes were averaged for the area where PT signals exceeded background level. PT spectra of plant tissues were calculated as an average of all of the signals around CNTs inclusion. Absolute values of PT signal were used to construct PT spectra.

Signals processing. For each laser pulse there were two signals acquired simultaneously: PA response (ultrasonic oscillations recorded by transducer) and PT signal (modulation of the probe beam intensity recorded by a photodiode). For each mapping step, PA/PT cytometer acquired and averaged 40 signals from 40 successive laser pulses.

PA signal processing. Time-gaiting was used to eliminate laser-caused electronic noise and the false signal from scattered light in transducer-recorded PA signals. The remaining part of the signal (from 3rd to 15th μs after the laser pulse) was recorded and digitally filtered with a bandpass filter to leave oscillations in the 750 kHz–4.5 MHz range only. The maximal amplitude of the acoustic oscillations in this range was considered as a desired PA signal representing the sample's response on the laser pulse. The PA map included two-dimensional coordinates of the irradiated sample spot and the corresponding PA signal amplitude.

PT thermal-lens signal processing. With the configuration selected, there were two typical shapes of PT thermal-lens signals observed: linear long positive signals and short nonlinear negative signals. Long positive signals (duration of signal ~30 μs), corresponding to the formation of linear thermal lens in the sample (focusing of the probe beam on refraction index gradient leading to increase in probe beam intensity), were associated with light absorption by the bulk of the sample, i.e., by the plant tissues. Short negative signals correspond to nonlinear processes emerging due to excessive heat generation and formation of nanobubbles around nanoparticles. A nanobubble defocuses or scatters probe light beam (decrease in probe beam intensity) and collapses in 0.2–7 μs.

Detection of the PT thermal-lens phenomenon in the sample is little affected by scattering of the probe beam or low frequency oscillations of its intensity. For processing PT data and calculation of thermal-lens strength, we used normalization of recorded photodiode readings on the level of probe beam intensity (not AC recording mode). Furthermore, we used relative change in probe beam intensity as a measure of thermal-lens effect. Recorded probe beam modulations normalized on initial probe beam intensity could be averaged in time domain and compared for different sample zones.

From each set of photodiode readings there were three signals determined: (*i*) probe beam intensity before laser pulse, I_0; and two curve parameters corresponding to expected types of thermal-lens signal; (*ii*) averaged level of photodiode readings in 8–9 μs interval, ΔI_{lin} (linear thermal-lens effect); and (*iii*) lower value of photodiode readings in 0–8 μs time interval after the laser pulse, ΔI_{neg}, (nonlinear bubbles effect).

To improve detection sensitivity, PT signals were processed as follows: for each photodiode reading set recorded for a laser pulse average value of 400 probe beam intensity readings were considered as I_0 value (duration of dataset recorded before laser pulse). Thereafter, all of the normalized photodiode readings curves, $\Delta I(t)$, recorded for the same sample spot were averaged in time domain (40 signals per spot). ΔI_{lin} linear thermal-lens signal was calculated from the averaged curve as an average of 200 photodiode readings corresponding to 8–9 μs interval after laser pulse. For description of fast signals from nanobubbles, we used curve smoothing with moving average trend for corresponding photodiode readings in 0–8 μs. ΔI_{neg} was calculated from this smoothed curve (smoothing period was selected to be much lower than that for linear signals: 20 signals = 0.1 μs in order not to degrade fast signal amplitude).

Statistical analysis. For continuous variables, the summaries included sample size, mean and standard deviation (or median and interquartile range), and minimum and maximum. For categorical variables, the summaries included frequencies and per-

centages. The coefficient of variation (i.e., Standard Deviation/Mean × 100) was calculated for each presented condition. All data were expressed as means ± SD. Differences among three or more groups were evaluated by means of one-way ANOVA test and independent-sample *t*-test performed for two-group comparisons. Analyses were conducted in statistical software SAS, and *P*-values of 0.05 or less were considered to indicate significance.

Detection of Carbon Nanotubes in Tomato Fruits of Plants Grown in Soil Supplemented with Multiwall Carbon Nanotubes. ***Experiment.*** The tomato plants (cv. Micro-Tom) were germinated from seeds in pots using a commercially available soil mix (*Sun Gro Redi-earth Plug and Seedlings Mix*, Sun Gro Horticulture, Inc.). All plants were grown in a growth chamber under 9 h light (26 °C) and 15 h dark (22 °C), 45% humidity and 500 μmol/m^2/s light intensity. The plants were watered once a day. Established young (three-week-old plants) were used for experiments with multiwall CNTs. For our experiments, tomato plants were divided into several groups containing eight plants each. The first group served as the control group, and control plants were grown as described above including watering with tap water. The second group contained plants that were germinated in a medium supplemented with CNTs (50 μg/mL), then transferred into soil pots and watered with tap water. The third group contained plants that were grown in soil containing CNTs. The fourth group contained plants that were germinated in agar medium containing CNTs in a concentration of 50 μg/mL; next, the seedlings were transferred into soil supplemented with CNTs. For the addition of CNTs to soil, we used water containing multiwall CNTs in a concentration of 50 μg/mL. The CNT-water solution (50 mL) was carefully added to the soil mix in each experimental pot. We carefully avoided direct contact of the CNT solution with the tomato plants. The plants were treated with CNTs once per week (each Wednesday). On other days of the week, these plants were watered only with tap water. Eight-week-old plants from all experimental groups produced green fruits which were collected and subjected for detection of CNTs inside fruits. For the preparation of samples, control green fruits and fruits from plants grown in soil supplemented with CNTs were ground in mortars. Each homogenized fruit was stabilized in a small amount of buffer (RLT buffer, Qiagen, Inc) supplemented with β-mercaptoethanol. RLT buffer-one fruit squash mix was spread in thin (almost transparent) films and analyzed using the Raman spectroscope. Raman scattering spectra were obtained with a Raman spectrometer (Horiba Jobin Yvon LabRam HR800) with 1,800 and 600 lines/mm gratings equipped and a Peltier-cooled CCD camera. Raman spectra were calibrated with standard silicon wafer using a specific peak of 521 cm^{-1} of the silicon. For all of the experiments, a 785 nm laser diode was used for excitation with power at the sample surface of 80 mW and a spot size of 1 μm. The scattered light was collected in the back-scattering geometry by a confocal Raman microscope on an Olympus BX-51 platform with 100× micro-objectives.

Raman spectroscopy for detection of nanoparticles in tomato fruits. Raman spectroscopy was used to detect the presence of multiwall CNTs in the fruits for the plants that were grown on CNT-containing medium only, CNT-containing soil only, and CNT-containing both medium and soil.

The Raman spectra of the multiwall CNTs contained several characteristic peaks: D band (ranging between 1,300 to 1,350 cm^{-1} which correspond to the defects in the graphitic structure; G band (ranging between 1,500 to 1,600 cm^{-1}) corresponding to the E_{2g} splitting for the graphitic structures; and finally the two-dimensional band (ranging between 2,600 to 2,700 cm^{-1}) which is a second order harmonic of the D band (1). Given the strong intensity of the G band, its intensity can be used for the detection and relative quantification of the CNT presence in the focal volume of the laser used for the Raman excitation. Although Raman spectroscopy is a relative method, it gives strong evidence for the presence of nanotubes in a particular sample and their relative concentration. Based on these considerations, it was found that the multiwall CNTs were able to reach the tomato fruits for all exposure conditions. Nonetheless, it is very difficult to completely compare the relative uptake amounts of the CNTs into fruits for those situations in which the CNTs were introduced at various stages of the plant developmental cycles, or when the nanotubes were exposed to the medium only, soil only, or combined into soil and medium. An interesting observation also supported by our PA/PT analysis is that the multiwall CNTs were found to form small agglomerates inside the fruit tissues. Furthermore, based on the relative intensity of the G band as acquired for the various situations, it was observed that the multiwall CNTs were up-taken into the tomato fruits in slightly larger amounts when the nanotubes were introduced into the medium only as compared to soil only. This observation can be explained by the more uniform CNT distribution in the medium as compared to the soil, where they can agglomerate and be transported by moisture away from the plant root system. As a result, it is suggested that soil conditions have a strong influence on the CNT ability to be uptaken by the plants, given variations in the pH and other chemical characteristics of the soil that could induce an agglomeration of the CNTs, which could result in large clusters that cannot be absorbed by the plants. Interestingly, it can be seen that the multiwall CNTs seem to be absorbed into the fruits/plants both from the medium, as well as from the soil (higher G band intensity for this case), through a continuous uptake process, indicating that the CNTs have the ability to penetrate the plant systems at various developmental stages. The presence of the CNTs in the fruit clearly indicates the considerable ability of the CNTs to distribute into all plant tissues.

1. Dresselhaus MS, Dresselhaus G, Saito R, Jorio A (2005) Raman spectroscopy of carbon nanotubes. *Phys Rep* 409:7–99.

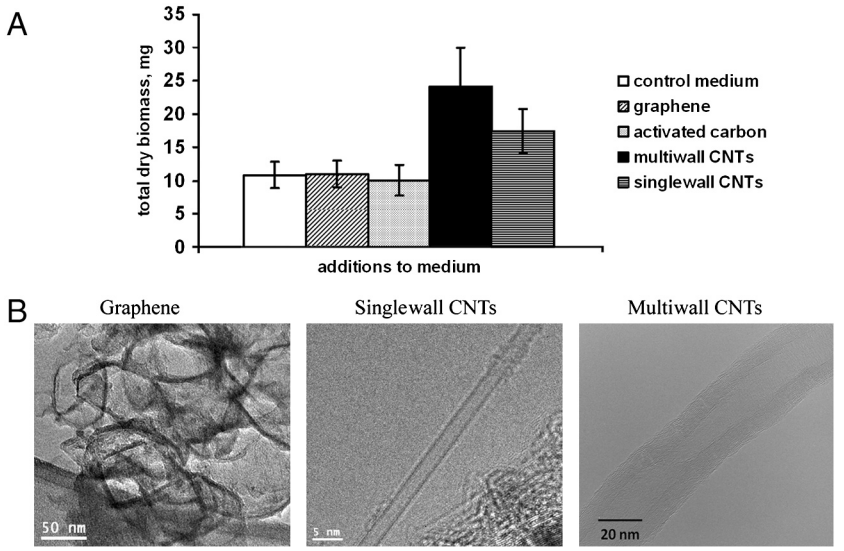

Fig. S1. (*A*) Effect of carbon materials on dry biomass accumulation of tomato plants. (*B*) High Resolution Transmission Electron Microscopy (HR-TEM) images of carbon nanomaterials used in our experiments: few layer graphene structures, single- and multiwall CNTs.

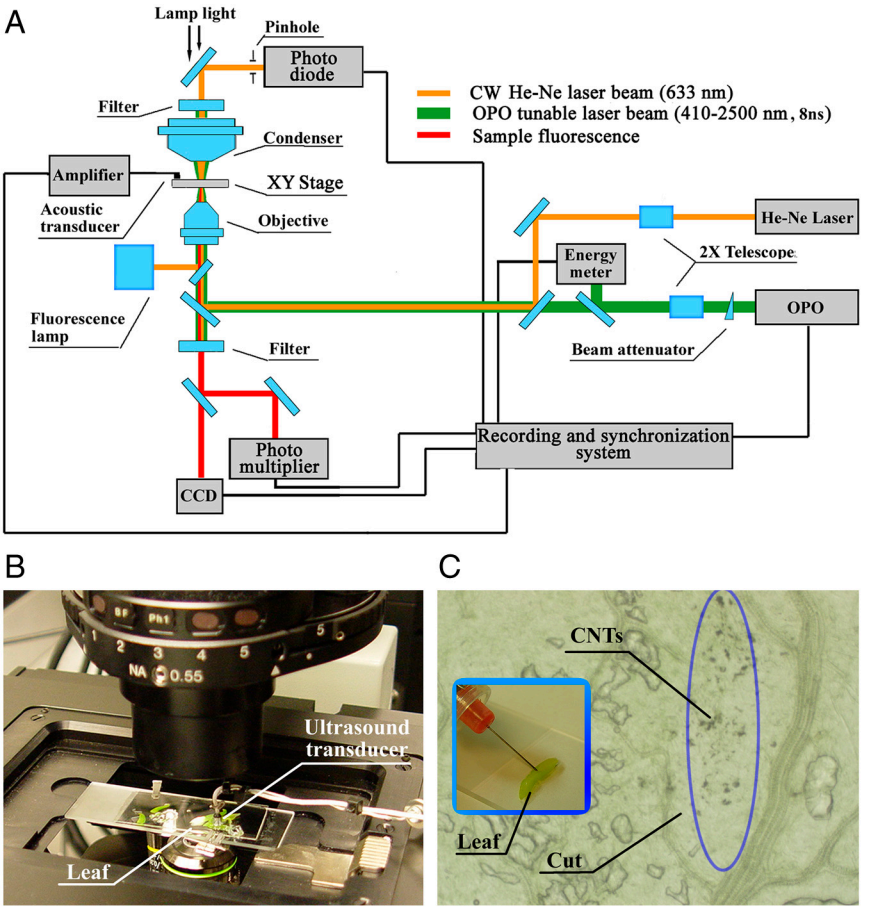

Fig. S2. (*A*) The integrated PA/PT cytometer schematic. (*B*) Tomato leaf placed between glass slides with the attached ultrasound transducer. (*C*) The local injection of multiwall CNTs into control tomato leaf for calibration purposes.

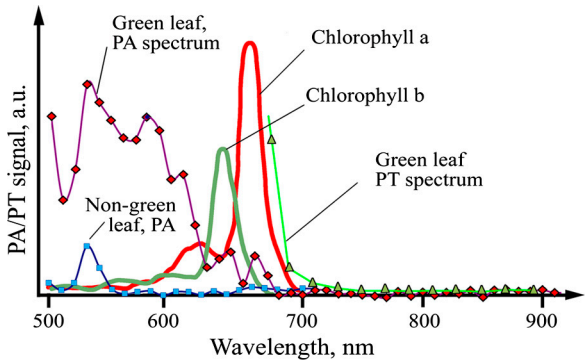

Fig. S3. PA and PT spectra of tomato leaves and absorption spectra of chlorophylls a and b Spectra were obtained from leaves of tomato plants grown in darkness with minimal chlorophyll production ("Nongreen leaf") and from plants exposed to light ("Green leaf"). Comparison of these samples with chlorophylls spectra reveals the nature of background absorption at wavelengths below 700 nm. Laser parameters: pulse energy, 30 μJ; tunable spectral range, 450–920 nm, diameter of laser beam, 2 μm.

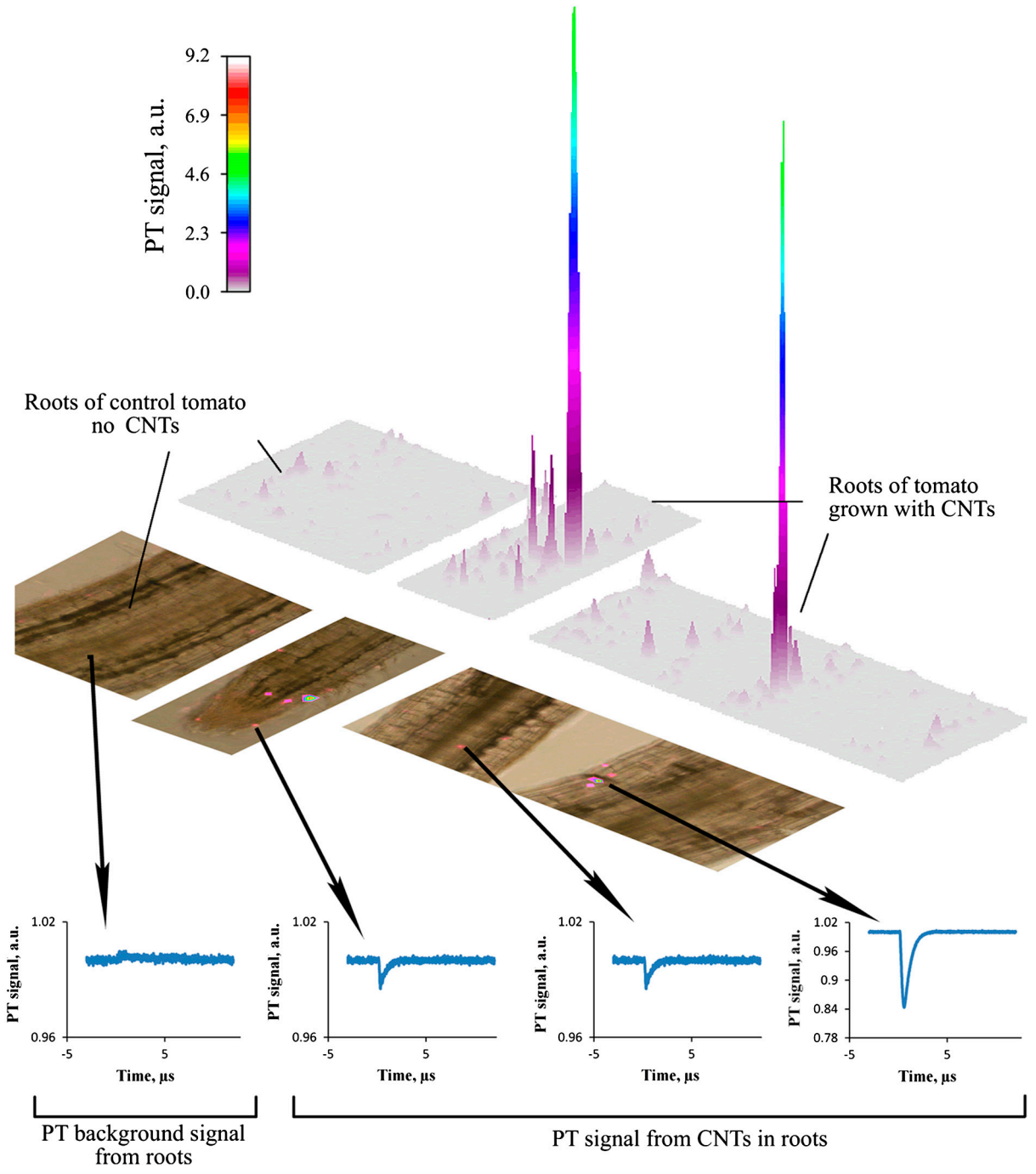

Fig. S4. Photothermal detection of multiwall CNTs in tomato roots. Conventional optical images in the bottom row are combined with PT images showing PT signals as rose spots. The insets show nonlinear PT signals from CNTs and linear PT signal from the control sample.

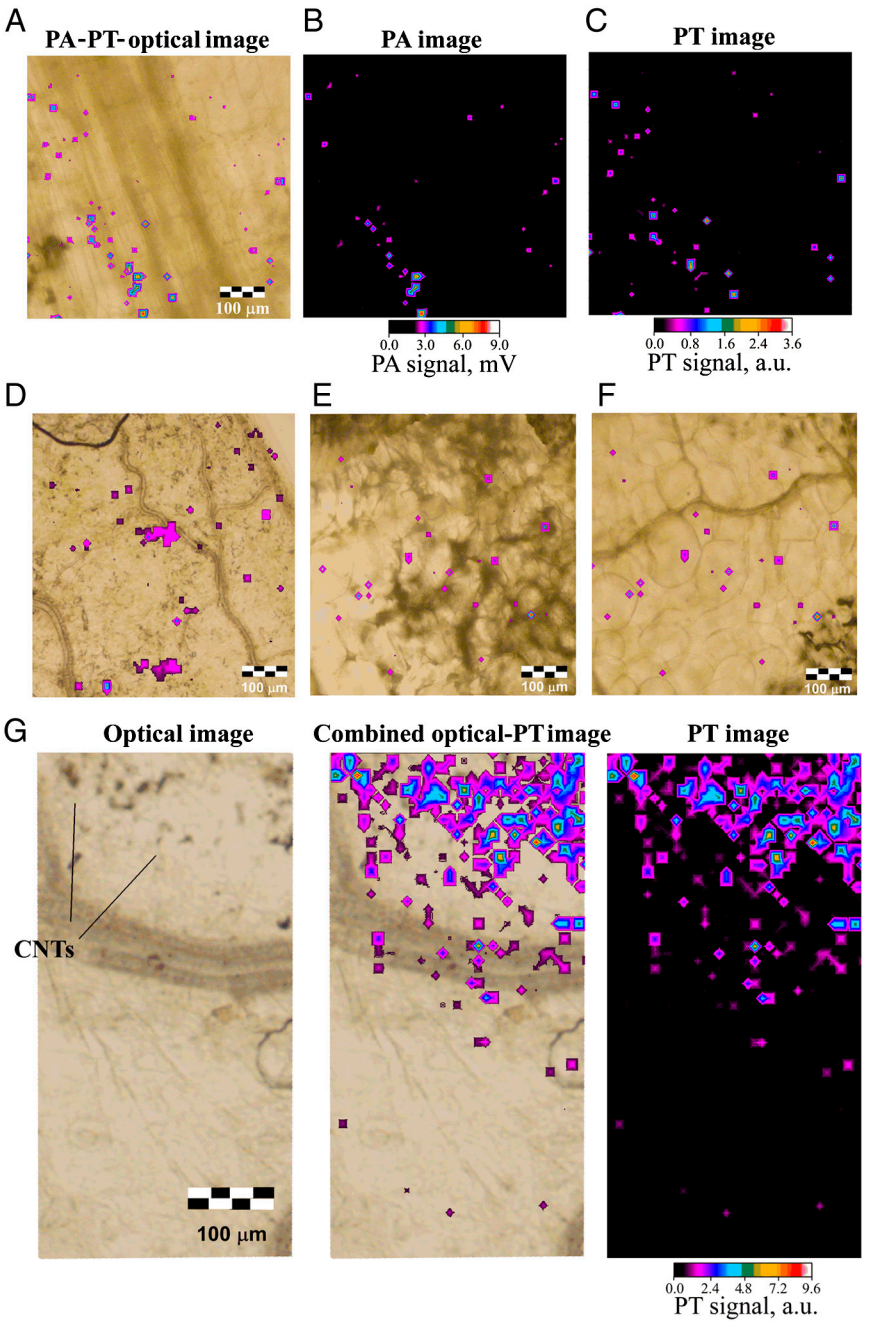

Fig. S5. PT/PA mapping of multiwall CNTs in tomato leaves. (*A*, *B*, and *C*) Simultaneous PA and PT detection of CNT distribution in tomato leaf; (*A*) represents combined PA-PT-optical image of the sample. (*A*, *D*, and *E*) Distribution of CNTs in tomatoes along the central vessel of the leaf (*A*, *D*) and at the edge of a leaf near small vessels (*E*). (*F*) Laser burning of leaf chromophores by intensive laser irradiation at 740 nm; comparison of images (*E* and *F*) reveals discoloring effects (i.e., removal of dark background) that allows better distinction of leaf vasculature. (*G*) Calibration of multiwall CNT imaging in tomato leaf with injected multiwall CNTs; the black structures visible in the leaf with optical imaging (left) correspond to injected nanoparticles; the combination of optical and PT images (center) reveals correlation of multiwall CNT images.

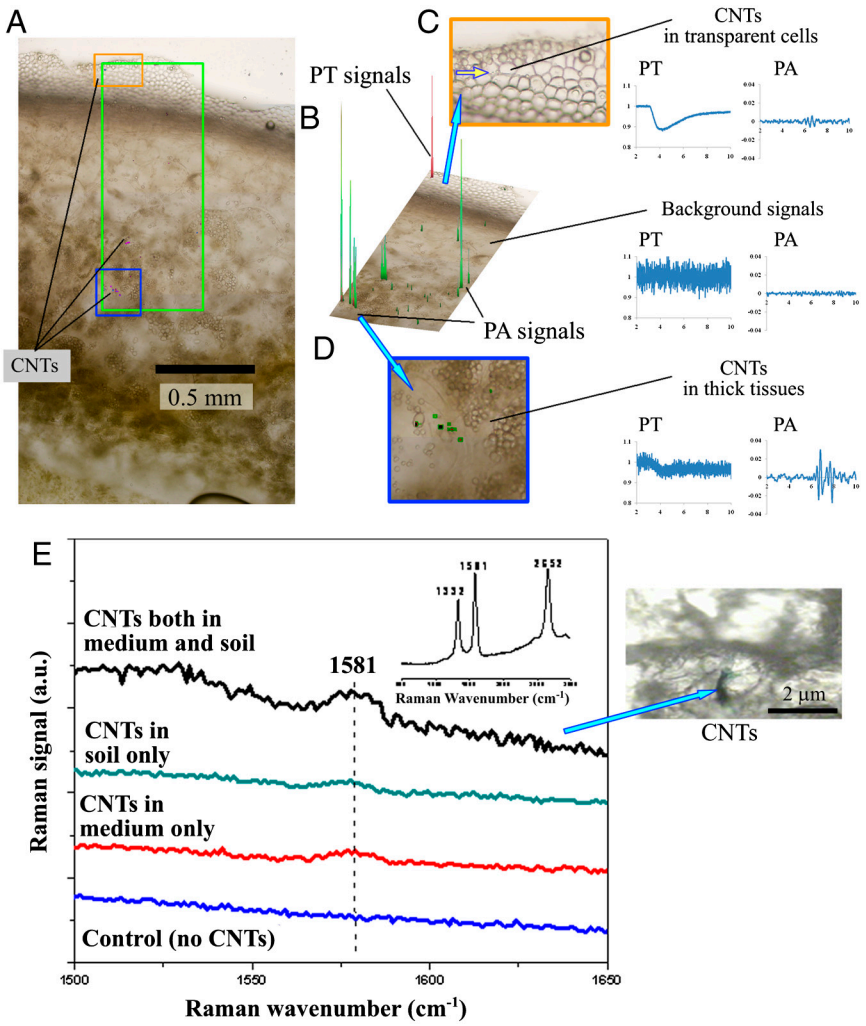

Fig. S6. (*A*) Multiwall CNT detection in 1 mm thick tomato fruit section. (*B*) Local intensive PA/PT signals from multiwall CNTs. (*C*) PT detection in transparent cells of tomato fruit; an arrow indicates the position of the acquired PT signals; however, no multiwall CNTs can be distinguished in thick, light scattering tissues. (*D*) PA detection sensitivity prevailed over that of PT mode in thick tissue. (*E*) Detection of CNTs inside tomato fruits by Raman method. Raman analysis of homogenized tomato fruits proved the presence of multiwall CNTs in the tomato fruits when the CNTs were introduced in the MS medium only, in the soil only, and both in the medium and soil (for details of experiment, see *SI Text*). The inset graph presents the Raman spectrum of the multiwall CNTs used for these studies. The analysis was conducted based on the intensity of the CNT G band. Each spectrum is the average of five measurements and was acquired with a 785 nm laser excitation and a power at the sample surface of 80 mW. The image on the right side is representative to the areas where the Raman analysis was done and shows the CNT agglomerations inside the homogenized fruit tissues prepared as described above, collected from plants that were exposed to multiwall CNTs both in the medium as well as in the soil.

Fig. S7. Transcript profile of CNTs specific (controls/tissues exposed to carbonaceous materials) differences in gene expression in leaf tissues of 10-day-old seedlings. Hierachical clustering (Euclidean distance) of log (2) fold changes over the average control (seedlings grown without carbon additions) fluorescence intensity. Two independent biological replicates for each treatment are presented here.

Abbreviations of samples:

0- tissues unexposed to carbonaceous materials;

AC-50- tissues exposed to activated carbon (50 ug/mL);

50- tissues exposed to multiwall carbon nanotubes (50 ug/mL);

100- tissues exposed to multiwall carbon nanotubes (100 ug/mL);

200- tissues exposed to multiwall carbon nanotubes (200 ug/mL).

Fig. S8. Transcript profile of CNTs specific (controls/tissues exposed to carbonaceous materials) differences in gene expression in root tissues of 10-day-old seedlings. Hierachical clustering (Euclidean distance) of log (2) fold changes over the average control (roots of seedlings grown without carbon additions) fluorescence intensity.

Two independent biological replicates for each treatment are presented here.

Abbreviations of samples:

0- tissues unexposed to carbonaceous materials;

AC-50- tissues exposed to activated carbon (50 ug/mL);

50- tissues exposed to multiwall carbon nanotubes (50 ug/mL);

100- tissues exposed to multiwall carbon nanotubes (100 ug/mL);

200- tissues exposed to multiwall carbon nanotubes (200 ug/mL).

Table S1. Involvement of genes affected by exposure to multiwall carbon nanotubes in tomato roots and leaves in specific biological processes

Description of biological process	No. of genes in roots	No. of genes in leaves
Reproduction	2	3
Carbohydrate metabolic process	2	5
Generation of precursor metabolites and energy	5	2
Nucleobase, nucleoside, nucleotide and nucleic acid metabolic process	10	4
DNA metabolic process	1	1
Transcription	5	12
Translation	4	1
Protein modification process	0	9
Cellular amino acid and derivative metabolic process	4	3
Lipid metabolic process	3	3
Transport	6	14
Response to stress	6	14
Cell cycle	0	2
Signal transduction	3	13
Cell-cell signaling	0	1
Multicellular organismal development	2	7
Behavior	1	
Metabolic process	10	15
Cell death	0	1
Catabolic process	7	11
Biosynthetic process	5	10
Response to external stimulus	1	3
Tropism	0	2
Response to biotic stimulus	1	4
Response to abiotic stimulus	3	15
Pollination	1	0
Pollen-pistil interaction	1	0
Response to extracellular stimulus	1	0
Photosynthesis	1	0
Anatomical structure morphogenesis	0	7
Response to endogenous stimulus	0	10
Embryonic development	1	1
Postembryonic development	1	6
Ripening	0	1
Flower development	1	4
Cellular process	9	29
Cellular homeostasis	4	0
Cellular component organization	7	6
Cell growth	1	2
Protein metabolic process	1	9
Secondary metabolic process	1	2
Cell differentiation	2	2
⟨⟩	9	17

The analysis was carried out by using Tomato Functional Genomics Database (http://ted.bti.cornell.edu/cgi-bin/TFGD/array/funcat.cgi). Analysis was done by using a list of CNTs-affected-genes generated by statistical analysis (*T*-test ($P < 10^{-3}$) based on log (2) fold changes of mRNA abundance over the average abundance of the specific transcript in the unexposed to carbon material seedlings.